Available online at www.sciencedirect.com
SCIENCE DIRECT®
Journal of Solid State Chemistry 177 (2004) 3245–3253
JOURNAL OF SOLID STATE CHEMISTRY
http://elsevier.com/locate/jssc

Anion substitution effects on structure and magnetism in the chromium chalcogenide Cr_5Te_8—Part I: Cluster glass behavior in trigonal $Cr_{(1+x)}Q_2$ with basic cell (Q = Te, Se; Te:Se = 7:1)

Zhong-Le Huang,[a,*] Wolfgang Bensch,[a] Diana Benea,[b] and Hubert Ebert[b]

[a] *Institute of Inorganic Chemistry, Christian-Albrechts-University Kiel, Olshausenstr. 40, D-24098 Kiel, Germany*
[b] *Department of Chemistry, LMU-Munich, Butenandstr. 5-13, D-81377 Munich, Germany*

Received 1 April 2004; received in revised form 18 May 2004; accepted 24 May 2004

Available online 20 July 2004

Abstract

The effect of substitution of the anion Te by Se in non-stoichiometric Cr_5Te_8 has been investigated with respect to its crystal structure, magnetic properties, and electronic structure. The compounds $Cr_{(1+x)}Q_2$ (Q = Te, Se; Te:Se = 7:1; $(1+x) = 1.234(6)$, 1.264(6), 1.300(7)) were synthesized at elevated temperatures followed by quenching the samples to room temperature. The crystal structures have been refined with X-ray powder diffraction data with the Rietveld method in the trigonal space group $P\bar{3}m1$ with lattice parameters $a = 3.8651(1)-3.8831(1)$ Å and $c = 5.9917(2)-6.0528(2)$ Å. The structure is related to the NiAs structure with full and deficient metal layers stacking alternatively along the c-axis. The irreversibility in the field-cooled/zero-field-cooled magnetization suggests that the substitution effects of one Te by one Se is strong enough to cause cluster-glass behavior, from ferromagnetic Cr_5Te_8 to cluster-glass $Cr_{(1+x)}Q_2$. Non-saturation magnetizations at 5.5 T and the magnetic relaxation results further support the existence of cluster-glass behavior. Accompanying SPR-KKR (spin-polarized relativistic Korringa–Kohn–Rostoker) band structure calculations strongly support the observation that the Cr(1) sites are preferentially occupied by Cr atoms and predict that these compounds are metallic. Results for the spin-resolved DOS and magnetic moments on each crystallographic sites are presented.

Keywords: Chromium chalcogenide; Anion substitution; Rietveld refinement; Low field magnetization; Cluster-glass; Relaxation; SPR-KKR; Band-structure calculations

1. Introduction

The study of chromium tellurides can be traced back to the discovery of ferromagnetism in 'CrTe' in 1930s [1]. In the binary chromium–tellurium system, the most extensive study is found in the region of the tellurium content between 50 and 62 at%. In this region, several well characterized phases with compositions $Cr_{(1-x)}Te$, Cr_3Te_4, Cr_2Te_3, and dimorphic Cr_5Te_8 were reported [2,3].

These phases all crystallize in the NiAs-type crystal structure with ordered metal vacancies [3]. Their structures consist of a distorted hexagonal close packing of Te atoms with Cr atoms in octahedral interstices. The Cr vacancies occur in every second metal layer, and thus the metal-deficient and metal-full layers stack alternatively along the c-axis. The distribution patterns of Cr vacancies depend not only on the Cr concentration but also on manners of the heat treatment used to prepare the samples. They are closely related to different structural modifications with deviations from hexagonal symmetry.

The magnetic studies show that binary tellurides are ferromagnetic with the Curie temperature T_c between 180 and 340 K, which decreases under high pressure [1,4,5(a)]. They show also metallic conductivity [5(a),6]. Band-structure calculations [5] demonstrate that the Cr 3d–Te 5p covalency and the Cr $3d_z^2$–Cr $3d_z^2$ overlap along the c-axis are the most important interactions in

*Corresponding author. Fax: +49-431-880-1520.
E-mail address: zlhuang@ac.uni-kiel.de (Z.-L. Huang).

0022-4596/$ - see front matter © 2004 Elsevier Inc. All rights reserved.
doi:10.1016/j.jssc.2004.05.046

CrTe, Cr_3Te_4 and Cr_2Te_3. The selenide analogue $Cr_{(1-x)}Se$ ($x = 0.875$) is antiferromagnetic [7a] and metallic [8] while Cr_3Se_4 and Cr_2Se_3 are antiferromagnets [7b–c] and semiconductors [8]. Some transition metal chalcogenides are found to be excellent candidates for half-metallic ferromagnets that are seen as a key ingredient in future high performance spintronic devices [9].

Recently, the crystal structures of the Cr_5Te_8 [3(f)] and Cr_5Se_8 [10(a)] phases were determined and it was found that the Cr_5Te_8 phase has a small existence range of tellurium content from 59.6 to 62.5 at%. For the lower Te content (from 59.5% to 61.5%), Cr_5Te_8 shows monoclinic symmetry and Te rich Cr_5Te_8 exhibits trigonal symmetry. In a previous study it was shown that the Cr_5Te_8 phases become ferromagnetic at low temperatures with a T_c strongly depending on the actual composition [11]. Cr_5Se_8 can only be prepared at high-pressure and high-temperature conditions [10]. Until now the magnetic ground states in these chalcogenides is not well understood. We note that Ti_5Te_8 which crystallizes in a trigonal system shows Pauli-paramagnetism [10(c)].

Based on the above facts and our previous study [3(f),10(a),11], we started to investigate the influence of the anion substitution by selenium and the cation substitution by titanium on the crystal structures and physical properties, especially magnetism, of the Cr_5Te_8 phases. It is reasonable to expect that different structural modifications and magnetic transitions from ferromagnetic to cluster-glass (CG), spin-glass (SG), or antiferromagnetism occur at different steps of substitution.

In this paper we first report on the effects of the anion substitution of Te by Se in the non-stoichiometric Cr_5Te_8 phases onto the crystal structure and magnetic properties. In particular we find a cluster-glass behavior in trigonal $Cr_{(1+x)}Q_2$ with basic cells (Q = Te, Se; Te:Se = 7:1; $(1+x) = 1.234$, 1.264, 1.300). The samples were prepared by the conventional ceramic method followed by quenching in cold water. The results of higher anion Se and cation Ti substitutions or by other heat treatments during the preparation of the samples that show different magnetic behavior like reentrant ferromagnetic, SG and CG will be published in following reports.

2. Experimental section

2.1. Synthesis

$Cr_{(1+x)}Q_2$ ($(1+x) = 1.234(6)$, 1.264(6), 1.300(7)) phases were prepared by the reaction of Cr (99.99%, Heraeus), Te (99.999%, Retorte) and Se (99.95%, Retorte) powders in evacuated silica tubes according to the composition range of Cr:Q = 4.60:8.00–5.50:8.00. Each starting mixture was heated up to 420°C and held at this temperature for 2 days. The temperature was then raised to 1000°C and kept at this temperature for 4–6 days. Finally the temperature was lowered to 800°C followed by quenching the samples into cold water.

2.2. Composition analysis

The Cr, Te, Se contents of the samples were determined by the inductively coupled plasma (ICP) technique. The compositions of the three samples are: $Cr_{1.228(6)}Te_{1.767(11)}Se_{0.233(2)}$, $Cr_{1.259(4)}Te_{1.764(2)}Se_{0.236(8)}$, and $Cr_{1.306(8)}Te_{1.767(13)}Se_{0.233(1)}$. These agrees well with the compositions determined by the full-pattern Rietveld refinements: $Cr_{1.234(6)}Q_2$, $Cr_{1.264(6)}Q_2$, and $Cr_{1.300(7)}Q_2$.

2.3. Powder X-ray diffraction and Rietveld refinement

X-ray powder patterns for the Rietveld refinements were collected on a STOE STADI P in transmission geometry using Cu$K\alpha$ radiation ($\lambda = 1.54056$ Å) in the 2θ-range of 10–100° with a position sensitive detector. The working voltage and current are 40 kV and 30 mA, respectively. The Rietveld refinements were done with the program package FULLPROF [12]. The background was interpolated by cubic splines between the selected points. The profile of the reflections was modeled with a pseudo-Voigt function (3 parameters). Preferred orientation was treated using March's function. The atomic coordinates were refined and the value for B_{iso} with a common variable for the Cr or Te/Se atoms. The position Cr(1) is fully occupied and Cr(2) is only partially occupied. Te and Se atoms are distributed statistically on the 2d site and the ratio of Te:Se was

Table 1
Crystal data and structure refinement parameters of $Cr_{(1+x)}Q_2$

Formula	$Cr_{(1+x)}Q_2$		
$(1+x)$	1.234(6)	1.264(6)	1.300(7)
Crystal system		Trigonal	
Space group	$P\bar{3}m1$		
a (Å)	3.8651(1)	3.8740(1)	3.8831(1)
c (Å)	5.9917(2)	6.0179(2)	6.0528(2)
V (Å^3)	77.516(6)	78.217(3)	79.040(5)
Z		1	
2θ range (deg)		10–100	
No. reflections	43	42	43
No. parameters	13	13	13
wR_p	5.35	5.57	5.67
R_e	4.38	4.60	4.83
GOF/χ^2	1.49	1.47	1.37
R_{Bragg}	4.48	2.75	3.14
R_F	4.87	3.32	3.77

Notes: The reliability factors values have the standard definitions.

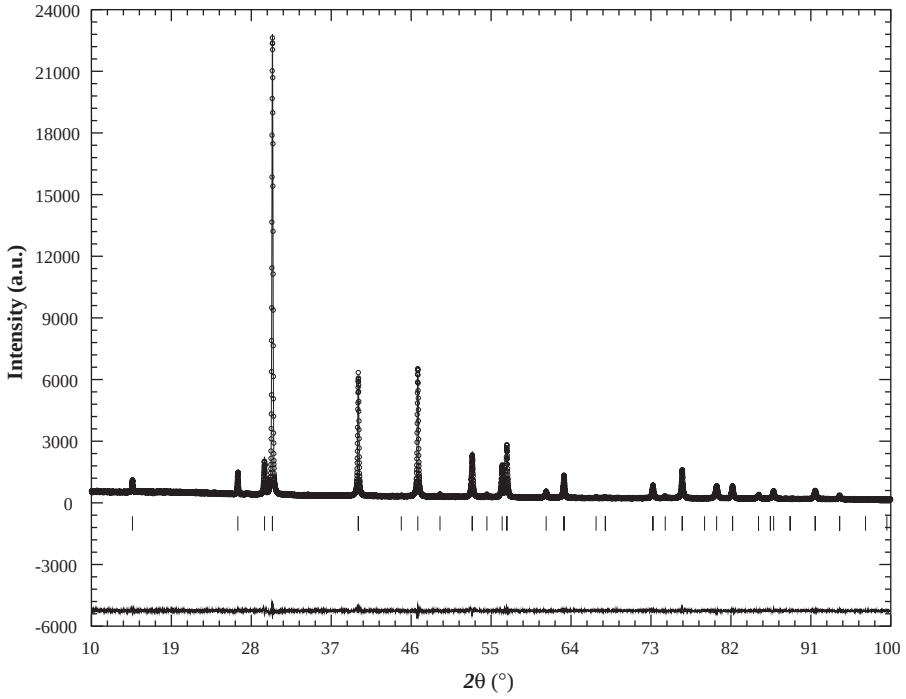

Fig. 1. Rietveld refinement plot for $Cr_{1.300(7)}Q_2$ with peak markers and difference plot at the bottom.

fixed at 7:1. In total 13 parameters were refined. The refinement results are listed in Table 1. Fig. 1 shows an example of the final Rietveld refinement plots for $Cr_{1.300(7)}Q_2$ with peak markers and difference plot at the bottom. Table 2 lists the atomic coordinates.

2.4. Magnetic measurements

Magnetic measurements were conducted with a Quantum Design MPMS-7 device. The DC susceptibilities were measured in the temperature range of $4\,K \leqslant T \leqslant 300\,K$ with a field of 1 T. The susceptibility of the samples was also measured from 300 to 600 K on a Faraday balance with an external field of 1.5 T. The zero-field cooled and field-cooled magnetizations M_{ZFC} and M_{FC} were taken as follows. The system was cooled in zero-field to 4.0 K, a field of 100 Oe was set immediately after $T = 4.0\,K$ was reached, and M_{ZFC} data taken on warming from 4.0 to 300.0 K; finally M_{FC} data recorded on cooling from 300.0 to 4.0 K with a field of 100 Oe. The field-dependent magnetizations were done at 4.0 K with a field up to 3.0 T or 5.5 T. The relaxation magnetizations were measured according to a well-defined $H-T$ procedure: the samples were field-cooled ($H = 1\,T$) from room temperature to 10 K, well lower than the freezing temperature T_f, and after temperature stabilization a waiting time of $t_w = 600\,s$ was followed. Thereafter the field was reduced to zero and the magnetization was recorded as a function of the elapsed time.

2.5. Band-structure calculations

The electronic structure of the $Cr_{(1+x)}Q_2$ system was calculated self-consistently by means of the spin polarized relativistic Korringa–Kohn–Rostoker (SPR-KKR) method in the atomic sphere approximation (ASA) mode [13–16]. The calculation method is based on the KKR-Green's function formalism that makes use of multiple scattering theory. The details of the calculation method have been described elsewhere [15,16]. Exchange and correlation effects were treated within the framework of local density functional theory, using the parametrization of Vosko et al. [17]. The coherent potential approximation (CPA) is used to describe the random distribution of Te/Se atoms within the chalcogen planes and the random distribution of the vacancies within the Cr layers [18,19].

3. Results and discussion

3.1. Crystal structure

The crystal structure of the trigonal $Cr_{(1+x)}Q_2$ phase is shown in Fig. 2(a). It can be viewed as a derivative of the hexagonal NiAs-type structure with metal vacancies. The Q atoms are hexagonal close packed and the Cr atoms occupy the octahedral interstices. We note that these trigonal phases have the same lattice parameters as the basic cell. The Q atoms have only one

Table 2
Atomic coordinates for $Cr_{(1+x)}Q_2$

Atom	x	y	z		B_{iso} (Å^2)	sof
$Cr_{1.234(6)}Q_2$						
Cr(1)	1*a*	0.00000	0.00000	0.00000	4.57(18)	1
Cr(2)	1*b*	0.00000	0.00000	0.50000	4.57(18)	0.234(18)
Te(1)	2*d*	0.33333	0.66667	0.2513(9)	3.64(6)	0.875
Se(1)	2*d*	0.33333	0.66667	0.2513(9)	3.64(6)	0.125
$Cr_{1.264(6)}Q_2$						
Cr(1)	1*a*	0.00000	0.00000	0.00000	4.21(15)	1
Cr(2)	1*b*	0.00000	0.00000	0.50000	4.21(15)	0.264(18)
Te(1)	2*d*	0.33333	0.66667	0.2520(8)	3.72(5)	0.875
Se(1)	2*d*	0.33333	0.66667	0.2520(8)	3.72(5)	0.125
$Cr_{1.300(7)}Q_2$						
Cr(1)	1*a*	0.00000	0.00000	0.00000	4.45(13)	1
Cr(2)	1*b*	0.00000	0.00000	0.50000	4.45(13)	0.300(21)
Te(1)	2*d*	0.33333	0.66667	0.2514(6)	4.08(5)	0.875
Se(1)	2*d*	0.33333	0.66667	0.2514(6)	4.08(5)	0.125

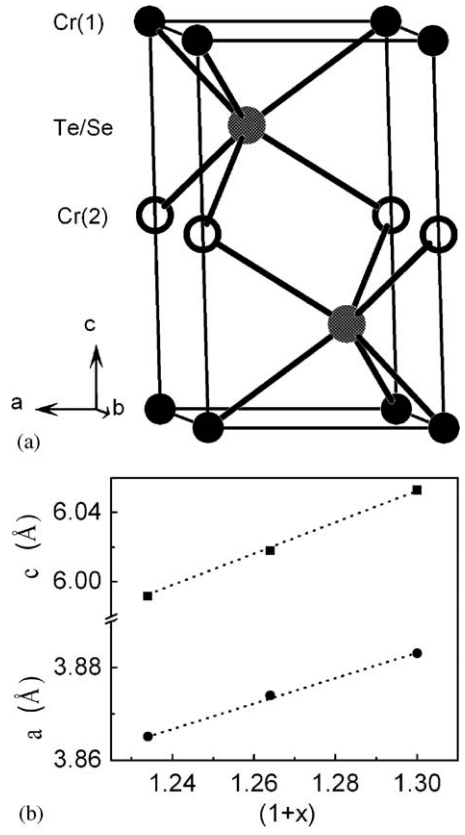

Fig. 2. (a) Crystal structure of $Cr_{(1+x)}Q_2$ and (b) dependences of cell parameters on chromium content in $Cr_{(1+x)}Q_2$. Dotted lines are used as guides for the eyes.

crystallographic site (2*d*), while there are two crystallographically unique positions for Cr atoms: Cr(1) on the 1*a* site and Cr(2) on the 1*b* site, respectively. Electron diffraction performed in a transmission electron microscope (TEM) confirms the absence of a crystallographic superstructure. So the Te/Se atoms are considered to be randomly distributed on the 2*d* site, forming the anion layers. For Cr atoms, there exists the question of site preference: do the Cr atoms occupy with the same occupancy the 1*a* and 1*b* sites or do they fill first the 1*a* site, and then, when this site is full, they occupy the 1*b* site? In order to answer the above questions, we have used several models for the Rietveld refinements. The three models listed in Table 3 are: (a) Cr atoms complete the 1*a* site, the remaining Cr atoms are on 1*b*; (b) some Cr atoms are moved from 1*a* to 1*b*; (c) Cr atoms are equally distributed on site 1*a* and 1*b*. Though there is no big difference for the different models, one can see that model (a) yields the best results. In fact, it is well documented from crystal field theory that the early transition metals have a great tendency to delocalize electrons by direct $t_{2g}-t_{2g}$ overlap thus favoring the occupation of sites in the full layers [20]. Further evidence for the site preference will be given by the total energy evaluation through the SPR-KKR band-structure calculations to be discussed in the last section.

Table 3
Results of the Rietveld refinements of different models for $Cr_{1.300(7)}Q_2$

Model	wR_p (%)	R_B (%)	R_F (%)	sof (Cr(1)/Cr(2))
a	5.67	3.14	3.77	1/0.30
b	5.81	3.25	4.77	0.76/0.54
c	6.20	4.04	6.01	0.65/0.65

sof is the site occupation factor.

The CrQ_6 octahedra in the crystal structure are quite regular. For $(1+x)=1.234(6)$, 1.264(6), and 1.300(7) the Cr(1)$-Q$ distances are 2.6921(10), 2.7022(10), 2.7097(9) Å and the Cr(2)$-Q$ bonds are 2.6832(10), 2.6890(10), 2.6999(9) Å, respectively. We note that the Cr(1)$-Q$ bond distances are longer than for Cr(2)$-Q$.

In an ionic picture, the electronic situation requires the coexistence of Cr^{3+} and Cr^{4+}; $Cr_{1.234}Q_2$, $Cr_{1.264}Q_2$ and $Cr_{1.300}Q_2$ may be written as $[Cr(1)^{3+}_{0.93}Cr(1)^{4+}_{0.07}Cr(2)^{4+}_{0.23}]Q_2$, $[Cr(1)^{3+}_{1.00}Cr(2)^{3+}_{0.04}Cr(2)^{4+}_{0.22}]Q_2$, $[Cr(1)^{3+}_{1.00}Cr(2)^{3+}_{0.20}Cr(2)^{4+}_{0.10}]Q_2$, respectively. In the *ab* plane, the CrQ_6 octahedra share common edges with Cr–Cr distance $d_{Cr(1)-Cr(1)}$ being equal to the value of cell parameter *a*. With the increase of Cr content, the parameter *a* and $d_{Cr(1)-Cr(1)}$ increase linearly, from 3.865 to 3.883 Å (Fig. 2(b)). Along the *c*-axis, the CrQ_6 octahedra share common faces. The Cr–Cr distance $d_{Cr(1)-Cr(2)}$ is equal to $\frac{1}{2}$ of the lattice parameter *c*. With increasing Cr content, the *c*-axis as well as the $d_{Cr(1)-Cr(2)}$ distance increase also linearly, from 2.996 to 3.026 Å for $d_{Cr(1)-Cr(2)}$ (Fig. 2(b)). In monoclinic Cr_5Te_8 [3(f)], the relevant Cr–Cr bond lengths across the common faces are 3.080 and 3.020 Å, and in trigonal Cr_5Te_8 [3(f)], they amount to 3.047 and 3.018 Å. Such short Cr–Cr distances suggest the existence of weak bonding interactions between the Cr atoms in neighboring layers.

The substitution of Te by Se in Cr_5Te_8 has led to the formation of trigonal $Cr_{(1+x)}Q_2$ with a small unit cell which may be regarded as the basic cell of the larger trigonal cell of Cr_5Te_8. It also introduces thus a different type of magnetic interaction through the Se atoms. The disorder of the Cr atoms in the metal deficient layers, and the randomness of Te and Se in the anion layers may generate magnetic frustration, thus introducing spin-glass or cluster-glass behavior in these materials as discussed below.

3.2. Magnetic properties

The temperature dependence of the inverse susceptibilities for $Cr_{(1+x)}Q_2$ ($(1+x)=1.234(6)$, 1.264(6), 1.300(7)) samples ($H=1$ T) are plotted in Fig. 3. In all cases, $\chi(T)$ obeys the Curie-Weiss law $\chi(T)=C/(T-\theta_P)$ in the temperature range of 200–300 K. The fitting parameters, the effective magnetic moment μ_{eff} and the Weiss constants θ_P are listed in Table 4. The effective magnetic moments μ_{eff} are between 4.10 and 4.34 μ_B per Cr atom, slightly larger than the expected value 3.87 μ_B for spin-only Cr^{3+}. In the temperature region between 300 and 600 K the magnetic moments per Cr atom is still large and amount to about 4.15 μ_B for the three different compounds. This is quite unusual for Cr^{3+}, but was often observed for chromium chalcogenides [21]. It may be due to the electron transfer from the *Q* to Cr through $d-p$ hybridization [22]. As pointed out above in an ionic picture of the compounds the coexistence of Cr^{3+} (d^3) and Cr^{4+} (d^2) is required, and one would assume that the effective magnetic moment is slightly smaller than 3.87 μ_B. The Weiss temperatures are quite large and positive, indicating strong ferromagnetic exchange interactions.

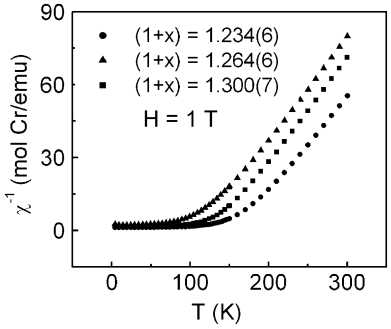

Fig. 3. Temperature dependencies of the inverse magnetic susceptibility of $Cr_{(1+x)}Q_2$ at field of 1 T.

In order to characterize the magnetic behavior of these compounds at low temperatures, the temperature dependence of zero-field-cooled (ZFC) and field-cooled (FC) magnetizations were measured. Fig. 4(a) shows the magnetizations M_{ZFC} and M_{FC}, respectively, for $Cr_{1.300(7)}Q_2$. For the zero-field-cooled magnetization, the curve shows a broad maximum at 86.0 K. For the field-cooled magnetization, it is nearly flat above 120 K and increases drastically with decreasing the temperature below 120 K. Finally, the magnetization tends to level off at lower temperature. Such a behavior is different from that for a canonical spin-glass. For spin-glasses, the FC curve is almost flat below the freezing temperature [23], but in our case it continues to rise. A similar behavior has been reported for cluster-glass (CG) materials like $La_{0.7}Sr_{0.3}Mn_{0.7}Co_{0.3}O_3$ [24(a)], $La_{0.5}Sr_{0.5}CoO_3$ [24(b), (c)], $Fe_{1/3}TiS_2$ [24(d)], $Ca_{0.9}Sm_{0.1}MnO_3$ [24(e)], and the molecule-based magnet $K_{1-2x}Co_{1+x}[Fe(CN)_6]\cdot yH_2O$ [24(f), (g)]. The rapid rise in magnetization at about 104 K may be associated with the occurrence of finite range ferromagnetic ordering, forming spin clusters near a quasi-critical temperature T_c, the clusters becoming randomly frozen as T is further decreased. Here we define the quasi-critical temperature or Curie temperature T_c and the freezing temperature T_f as follows (Fig. 4(b)): T_c is the temperature where the minimum of the $d\chi_{(ZFC)}/dT$ vs. T curve occurs, while T_f is the temperature at which $(d\chi_{(ZFC)}/dT)$ crosses the zero line. We note that the ZFC and FC magnetizations for the other samples which are not shown here have similar profiles. Their Curie temperature T_c and the freezing temperatures T_f are listed in Table 4. Note that for $Cr_{1.264(6)}Q_2$ the lowest values for T_c and T_f are observed. This observation should be related to the ratio of the number of chromium atoms distributed over the vacancies and their specific local distribution in the metal-deficient layers, though the full understanding is still not unveiled.

An example of the field dependence of magnetization $M(H)$ is shown for $Cr_{1.300(7)}Q_2$ in Fig. 5(a). Again the

Table 4
Magnetic parameters for $Cr_{(1+x)}Q_2$

$(1+x)$	μ_{eff} (μ_B/Cr-atom)	θ_P (K)	T_c (K)	T_f (K)	M_{rem} (μ_B/Cr-atom)	M_{max} (μ_B/Cr-atom)	H_c (T)
1.234[a,b]	4.10	158	109.0	84.0	0.73	1.45	0.200
1.264[a]	4.31	115	69.0	57.0	0.25	1.12	0.0175
1.300	4.34	133	104.0	86.0	0.35	1.58	0.0313

[a] $M-H$ curves with a field up only to 3 T.
[b] $M-H$ curve from a new sample without former magnetic treatment history.

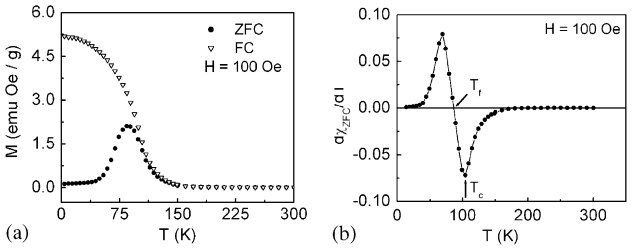

Fig. 4. (a) Temperature-dependent M_{ZFC} and M_{FC} for $Cr_{1.300(7)}Q_2$ with a field of 100 Oe and (b) $[d\chi_{(ZFC)}/dT]$ as a function of temperature for $Cr_{1.300(7)}Q_2$ with a field of 100 Oe.

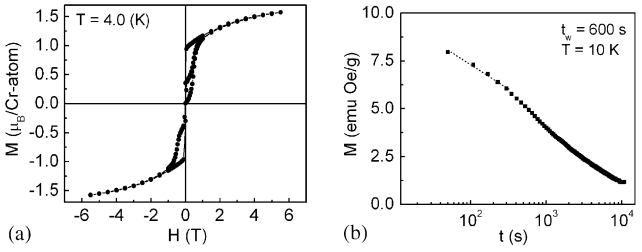

Fig. 5. (a) Field-dependent magnetization for $Cr_{1.300(7)}Q_2$ at 4.0 K. (b) Thermoremanent magnetization relaxation for $Cr_{1.234(6)}Q_2$ at $T = 10$ K and with $t_w = 600$ s.

compounds $Cr_{1.234(6)}Q_2$ and $Cr_{1.264(6)}Q_2$ have similar curves. The remanent moments M_{rem}, the coercive fields H_c, and the magnetic moments M_{max} at a field of 3 T or 5.5 T are listed in Table 4. Here one notifies that the coercive fields are small for all compounds, consistent with their high chromium site symmetries in their crystal structures. From Fig. 5(a) and Table 4, one finds that the magnetic moments M_{max} at a field up to 3 or 5.5 T are between 1.1 and 1.6 μ_B/Cr. They are smaller than the expected value of 3.0 μ_B for Cr^{3+}. This may be considered as another indication for the existence of spin-glass like or cluster-glass behavior, in which the saturation can never be reached.

The existence of the cluster-glass behavior has been further confirmed by the time-dependent magnetization relaxation using a measuring process according to a well-defined $H-T$ procedure [23]. Fig. 5b shows an example of the relaxation results for $Cr_{1.234(6)}Q_2$. From this figure, one finds that the decay of the remanent magnetization is remarkably fast (decrease of about

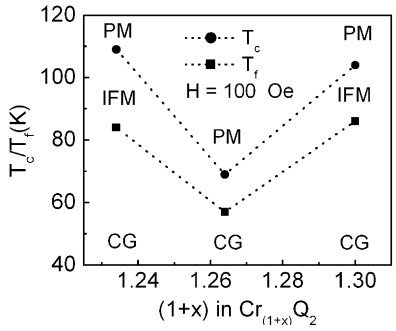

Fig. 6. Magnetic phase diagram. Dotted lines are used as guides for the eyes. PM: paramagnetism; CG: cluster-glass; IFM: intra-cluster ferromagnetism or short-ranged FM ordering, i.e., the formation of clusters.

87% after 3 h at 10 K), indicative of a non-equilibrium nature of the system. For $t \gg t_w$, the data can be fitted to a logarithmic time dependence. Our data show no minimum in the relaxation rate S $[S = dM/d(\ln t)]$ at $t = t_w$, in contrast to that of a canonical spin-glass [23], but similar to data reported for the cluster-glass compounds $La_{0.5}Sr_{0.5}CoO_3$ [24(b), 24(c)], U_2RhSi_3 [24(h)], and for the molecule-based magnet $K_{1-2x}Co_{1+x}[Fe(CN)_6]\cdot yH_2O$ [24(f), 22(g)].

Using the Curie temperature T_c and the freezing temperature T_f, the magnetic phase diagram for $Cr_{(1+x)}Q_2$ is constructed and it is shown in Fig. 6. From this figure, one can distinguish three regions. In the high temperature region paramagnetic behavior is observed. In the low temperature region cluster-glass properties occur and in the intermediate intra-cluster ferromagnetism or short-range ferromagnetic ordering is present, i.e., the formation of clusters.

In conclusion, our results suggest that $Cr_{(1+x)}Q_2$ ($(1+x) = 1.234(6)$, $1.264(6)$, $1.300(7)$) phases exhibit cluster-glass behavior at low temperatures, with short-range ordering within clusters, and with strong interaction among clusters. Such an observation is in full agreement with the structural characteristics of the Se substituted compounds. First, in these compounds exist a partial disorder of chromium atoms over the 1*b* site and the partial occupancy and randomness of Te and Se atoms on the 2*d* site; and secondly among the Cr–Cr ferromagnetic interaction through the common faces (Te layers), the substitution of Te by Se introduces an

antiferromagnetic interaction component due to the shorter Cr–Cr separation and stimulates the competition between ferromagnetic and antiferromagnetic interactions, i.e. the frustration. The coexistence of disorder and frustration thus leads to a magnetically disordered state, i.e., a cluster-glass. From a formal point of view the electronic situation requires the coexistence of Cr(III) d^3 and Cr(IV) d^2. Hence, a double-exchange mechanism should also be considered leading to ferromagnetic exchange interactions. Furthermore, according to the band structure calculations the compounds are metals (see below) and the cluster-glass behavior may be due to the RKKY mechanism.

3.3. Band-structure calculations

3.3.1. Preferential site occupation

The SPR-KKR band structure calculations have been performed for the quenched ferromagnetic samples $Cr_{(1+x)}Q_2$ ($(1+x)=1.23$, 1.26, 1.30). The structure and the lattice parameters used for these calculations are those determined by experiment, as it is described in Section 2. The X-ray powder diffraction data concerning the site occupation in the $Cr_{(1+x)}Q_2$ phases is questioned in Section 3.1. According to the Rietveld refinements, the layer of Cr at $z=0$ denoted by Cr(1) is fully occupied, whilst the plane of Cr(2) at $z=\frac{1}{2}$ is only partially occupied.

The preference of Cr atoms for one of the layers must be energetically determined and it must be reflected in the variation of the total energy if a certain percentage of Cr is moved from Cr(1) to the Cr(2) layer. In order to verify this assumption, the variation of the total energy of the system is calculated when y% of the Cr(1) atoms are moved to the Cr(2) plane, according to the scheme: $Cr(1)_{1.0}Cr(2)_{0.30}Q_2 \rightarrow Cr(1)_{(1.0-y)}Cr(2)_{(0.30+y)}Q_2$. As can be seen in Fig. 7, an increase in the total energy of the $Cr_{1.30}Q_2$ system results when moving Cr atoms from the Cr(1) to the Cr(2) planes. This increase of the total energy with the concentration y is monotonous. This result clearly confirms that the Cr atoms preferentially occupy the Cr(1) sites. If the overall Cr concentration would increase in this system, the Cr(1) plane would be occupied first. Only after the Cr(1) plane has been fully occupied, the Cr atoms start to populate the Cr(2) plane. The results of the calculations for the $Cr_{1.23}Q_2$ and $Cr_{1.26}Q_2$ systems lead to the same conclusion.

3.3.2. Density of states and magnetic moments

The spin-resolved density of states for the system $Cr_{1.30}Q_2$ is presented in Fig. 8. The main features of the KKR calculated DOS of these systems are similar to the results of ASW calculations reported by Dijkstra et al. [5(a)], [5(b)] for stoichiometric CrTe and CrSe compounds with a NiAs-like structure. One should note that for the SPR-KKR density of states representation

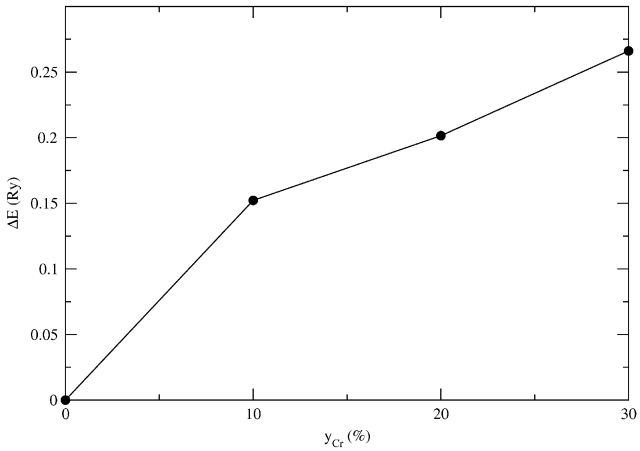

Fig. 7. The SPR-KKR total energy variation of the system $Cr_{1.30}Q_2$ as a function of chromium concentration y moved from site a to site b, according to the scheme: $Cr(1)_{1.00}Cr(2)_{0.30}Q_2 \rightarrow Cr(1)_{(1-y)}Cr(2)_{(0.30+y)}Q_2$.

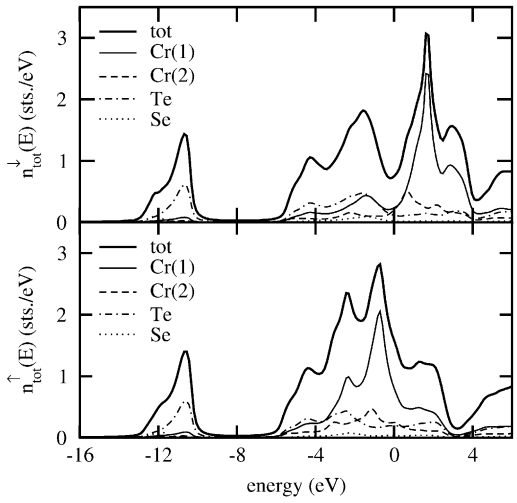

Fig. 8. Spin-resolved DOS of the system $Cr_{1.300}Q_2$ by SPR-KKR calculations. The origin of the energy scale is E_F.

for non-stoichiometric compounds each component is weighted by its concentration in order to get the total DOS.

The band at around 12 eV binding energy has anion s-character, whilst the higher energy band crossing the Fermi level has Cr 3d–Te/Se p character. In the lower part of the $d-p$ band, the p-character is obvious and the influence of the exchange-splitting is minor. The higher part of the $d-p$ band, having a Cr 3d character shows a clear exchange-splitting. The difference in DOS between the systems of the type $Cr_{(1+x)}Q_2$ with different Cr content appears in exchange-splitting and in the separation of the $p-$ and d-like peaks in the $d-p$ band.

The magnetic moments for $Cr_{(1+x)}Q_2$ obtained by SPR-KKR band structure calculations are presented in

Table 5
Spin and orbital magnetic moments in trigonal $Cr_{1+x}Q_2$ non-stoichiometric compounds

	$Cr_{1.23}Q_2$		$Cr_{1.26}Q_2$		$Cr_{1.30}Q_2$	
	m_{spin} (μ_B)	m_{orb} (μ_B)	m_{spin} (μ_B)	m_{orb} (μ_B)	m_{spin} (μ_B)	m_{orb} (μ_B)
Cr(1)	2.9536	0.0112	2.9972	0.0113	3.0422	0.0111
Cr(2)	2.2440	0.0231	2.3494	0.0231	2.5016	0.0226
Te	−0.1929	−0.0077	−0.1949	−0.0083	−0.1943	−0.0093
Se	−0.2797	−0.0025	−0.2821	−0.0032	−0.2810	−0.0042

Table 5. As can be seen, the magnetic moments of Cr on Cr(2) are about 25% smaller than those on Cr(1) sites. This observation supports the ionic picture where the mixed valence states of Cr^{3+} and Cr^{4+} coexist and Cr^{4+} has the priority to occupy the Cr(2) 1*b* site. With the increase of Cr content, the magnetic moments in both Cr(1) and Cr(2) increase simultaneously. This enhancement is more pronounced for Cr(2) than for Cr(1) magnetic moments. When the Cr content in the system $Cr_{(1+x)}Q_2$ increases from $Cr_{1.23}Q_2$ to $Cr_{1.30}Q_2$, the magnetic moment of Cr(1) increase by around 3%, whilst that for Cr(2) increase by around 10%. We should note also the magnitude and the sign of the magnetic moment on the chalcogen atoms. Their magnetic moments are antiparallel to the Cr moments and almost independent on the Cr content. This negative magnetic polarization is explained by Dijkstra et al. [5(a)] in the case of Cr–Te compounds by covalent mixing of Cr 3*d* and Te *p*-bands. This explanation can be extended to $Cr_{(1+x)}Q_2$ compounds if we take into account the calculated DOS of $Cr_{(1+x)}Q_2$ systems which show a slight displacement of the Te/Se spin-up *p*-bands, in agreement with the picture of Dijkstra et al. [5(a)].

4. Conclusion

The concept of chemical substitution has been successfully used to synthesize the quasi-binary $Cr_{(1+x)}Q_2$ phases, in which chromium atoms are located in full and deficient metal layers stacking alternatively in the *c* direction, and Se and Te atoms are distributed statistically in the anion layers. The substitution of one Te by one Se atom in Cr_5Te_8 has introduced the disorder in the anion layers and antiferromagnetic interaction among chromium atoms through the Se bridges, thus creating frustration in the 3D lattice. Ferromagnetic Cr_5Te_8 thus changes to cluster-glass $Cr_{(1+x)}Q_2$, accompanied by the decrease of the Curie temperature. SPR-KKR band-structure calculations confirm the observation of preferential site occupation of Cr atoms in the 1*a* site from the Rietveld refinements and show that these compounds are metallic.

Syntheses using the high temperature route followed by slow cooling leads to trigonal $Cr_{(5+x')}Q_8$ phases with superstructures. Studies of compounds with a higher degree of Se substitution are in progress. Preliminary results of Ti substitution in Cr_5Te_8 show a very rich magnetic behavior like reentrant ferromagnetic phenomenon, spin-glass, cluster-glass with ferromagnetic or antiferromagnetic interactions. They will be reported in forthcoming papers.

Acknowledgments

The authors thank Dr. H. Pausch (University of Kiel) for his help in magnetic measurements and Mr. H. Hartl (LMU-Munich) for chemical analysis (ICP). The DFG is acknowledged for the financial support of SPP 1136 project (BE 1653/12-1).

References

[1] (a) H. Haraldsen, E. Kowalski, Z. Anorg. Allgem. Chem. 224 (1935) 329–336;
(b) H. Harldsen, A. Neuber, Z. Anorg. Allgem. Chem. 234 (1937) 353–371.
[2] (a) H. Ipser, K.I. Komarek, K.O. Klepp, J. Less-Common Met. 92 (1983) 265–282;
(b) G. Chattopadhyay, J. Phase Equilibria 15 (4) (1994) 1–4.
[3] (a) H. Ido, K. Shirakawa, T. Suzuki, T. Kanedo, J. Phys. Soc. Japan 26 (1969) 663–665;
(b) G.I. Makovetskii, A.I. Galyas, G.M. Severin, K.I. Yanushkevich, Inorg. Mater. (USSR) (see: Izv. Akad. Nauk, Neorg. Mater.) 32 (1996) 960–964;
(c) A.F. Andresen, Acta Chem. Scand. 17 (1963) 1335–1342;
(d) A.F. Andresen, Acta Chem. Scand. 24 (1970) 3495–3509;
(e) T. Hamasaki, T. Hashimoto, Y. Yamaguchi, H. Watanabe, Solid State Commun. 16 (1975) 895–897;
(f) W. Bensch, O. Helmer, C. Naether, Mater. Res. Bull. 32 (1997) 305–318.
[4] (a) K. Ozawa, T. Yoshimi, M. Irie, S. Yanagisawa, Phys. Stat. Sol. 11 (1972) 581–588;
(b) J.M. Leger, J.P. Bastide, Phys. Stat. Sol. 29 (1975) 107–113;
(c) M. Yuzuri, T. Kanomata, T.J. Kaneko, J. Magn. Magn. Mater. 70 (1987) 223–224;
(d) K. Hatakeyama, T. Kaneko, H. Yoshida, S. Ohta, S. Anzai, J. Magn. Magn. Mater. 90–91 (1990) 175–176;
(e) T. Kanomata, Y. Sugawara, K. Kamishima, H. Mitamura, T. Goto, S. Ohta, T. Kaneko, J. Magn. Magn. Mater. 177–181 (1998) 589–590.
[5] (a) J. Dijkstra, H.H. Weitgering, C.F. van Bruggen, C. Haas, R.A. de Groot, J. Phys.: Condens. Matter 1 (1989) 9141–9161;
(b) J. Dijkstra, C.F. van Bruggen, C. Haas, R.A. de Groot, J. Phys.: Condens. Matter 1 (1989) 9163–9174.

[6] M. Chevreton, M. Murat, E.F. Bertaut, Collogque CNRS 157 (1965) 49–53.
[7] (a) F.K. Lotgering, E.W. Gorter, J. Phys.: Chem. Solids. 3 (1957) 238–249;
(b) A. Maurer, G.J. Collin, J. Solid State Chem. 34 (1980) 23–25;
(c) Y. Adachi, M. Ohashi, T. Kaneko, M. Yuzuri, Y. Yamaguchi, S. Funahashi, Y. Morii, J. Phys. Soc. Japan 63 (1994) 1548–1559.
[8] M. Chevreton, M. Murat, C. Eyraud, E.F. Bertaut, Le J. Phys. 24 (1963) 443–446.
[9] W.H. Xie, Y.Q. Xu, B.G. Liu, D.G. Pettifor, Phys. Rev. Lett. 91 (2003) 037204-1037204-4.
[10] (a) H. Huppertz, H. Luehmann, W. Bensch, Z. Naturforsch. 58b (2003) 934–938;
(b) A.W. Sleight, T.A. Bither, Inorg. Chem. 8 (1968) 566–569;
(c) K. Hatakeyama, A. Takase, S. Anzai, H. Yoshida, T. Kaneko, S. Abe, S. Ohta, Jpn. J. Appl. Phys. 39 (2000) 507–510.
[11] K. Lukoschus, S. Kraschinski, C. Naether, W. Bensch, J. Solid State Chem. 177 (2004) 951–959.
[12] J. Rodriguez-Carvajal, Fullprof. 2k, Version 2.0c—July 2002/ Lab. Leon Brillouin (2002).
[13] J. Korringa, Physica 13 (1947) 392–400.
[14] W. Kohn, N. Rostoker, Phys. Rev. 94 (1954) 1111–1120.
[15] H. Ebert, et al., The Munich SPR-KKR package, version 2.1.1, http://olymp.cup.uni-muenchen.de/ak/ebert/SPRKKR/
[16] H. Ebert, in: H. Dreyssé (Ed.), Electronic Structure and Physical Properties of Solids, Springer, Berlin, 2000, pp. 191–246.
[17] S.H. Vosko, L. Wilk, M. Nusair, Can. J. Phys. 58 (1980) 1200–1211.
[18] P. Soven, Phys. Rev. 156 (1967) 809–813.
[19] G.M. Stocks, W. Temmerman, B.L. Györffy, Phys. Rev. Lett. 41 (1978) 339–343.
[20] (a) A.V. Powell, D.C. Colgan, C. Ritter, J. Solid State Chem. 134 (1997) 110–119;
(b) J.B. Goodenough, Magnetism and the Chemical Bond, Wiley, New York, 1963.
[21] (a) W. Bensch, B. Sander, O. Helmer, C. Näther, F. Tuczek, A.I. Shames, A.M. Panish, J. Solid State Chem. 145 (1999) 235–246;
(b) W. Bensch, B. Sander, R.K. Kremer, W. Kockelmann, J. Solid State Chem. 158 (2001) 198–207.
[22] K. Shimada, T. Saitoh, H. Namatame, A. Fujimori, S. Ishida, S. Asano, S. Anzai, Phys. Rev. 53 (1996) 7673–7683.
[23] J.A. Mydosh, Spin Glasses: an Experimental Introduction, Taylor & Francis, London, 1993.
[24] (a) X.G. Li, X.J. Fang, G. Ji, W.B. Wu, K.H. Wong, C.L. Choy, H.C. Ku, J. Appl. Phys. 85 (1999) 1663–1666;
(b) S. Mukherjee, R. Ranganathan, P.S. Anikumar, P.A. Joy, Phys. Rev. B 54 (1996) 9267–9274;
(c) D.N.H. Nam, K. Jonason, P. Nordblad, N.V. Khiem, N.X. Phuc, Phys. Rev. B 59 (1999) 4189–4194;
(d) M. Koyano, M. Suezawa, H. Watanabe, M. Inoue, J. Phys. Soc. Japan 63 (1994) 1114–1122;
(e) A. Maignan, C. Martin, F. Damay, B. Raveau, Phys. Rev. B. 58 (1998) 2758–2763;
(f) D.A. Pejakovic, J.L. Manson, J.S. Miller, A.J. Epstein, J. Appl. Phys. 87 (2000) 6028–6030;
(g) D.A. Pejakovic, J.L. Manson, J.S. Miller, A.J. Epstein, Phys. Rev. Lett. 85 (2000) 1994–1997;
(h) D.X. Li, A. Donni, Y. Kimura, Y. Shiokawa, Y. Homma, Y. Haga, E. Yamamoto, T. Honma, Y. Onuki, J. Phys.: Condens. Matter. 11 (1999) 8263–8274.